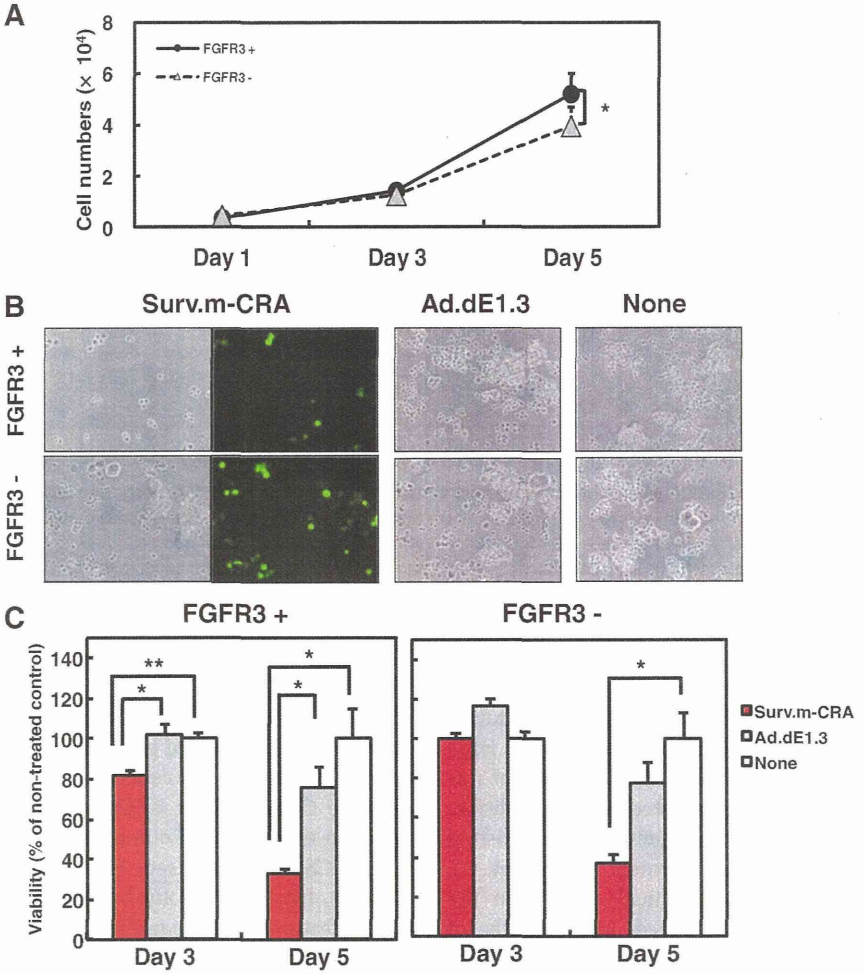

Figure 6 Viral replication of Surv.m-CRA and cytotoxicity against sorted FGFR3-positive and FGFR3-negative cells. (A) Growth curves of sorted cells. Whereas FGFR3-positive cells proliferated somewhat more rapidly than FGFR3-negative cells, the difference was not drastic. *, $P < 0.05$. **(B)** Representative images of phase-contrast and the fluorescence-microscopic pictures 5 days after infection with Surv.m-CRA, Ad. dE1.3, or no virus. Whereas viral replication and cytopathic effects of Surv.m-CRA were prominent in both groups, the proportion of remaining cells 5 days after Surv.m-CRA infection at an MOI of 1 was lower in sorted FGFR3-positive cells than in sorted FGFR3-negative cells. **(C)** Cell viability was determined by WST-8 assay 3 or 5 days after infection. Cytotoxic effects of Surv.m-CRA were statistically significantly higher than those of Ad. dE1.3 solely in the sorted FGFR3-positive cells. *, $P < 0.05$; **, $P < 0.005$ between Surv.m-CRA and either Ad.dE1.3 or no virus.

induced prominent viral replication and cell death in all rhabdomyosarcoma cell fractions, including RSCs, and that such effects were more potent in RSCs than in progeny. This is consistent with the higher survivin expression levels and promoter activities in RSCs relative to progeny, shown above (Figure 3).

Surv.m-CRA had potent *in vivo* therapeutic effects on tumors generated from RSC-enriched rhabdomyosarcoma cells in mice

We subcutaneously inoculated RSC-enriched rhabdomyosarcoma cells into mice to generate a tumor nodule, into which Surv.m-CRA (1×10^9 pfu), the control Ad. dE1.3, or no virus (none) was subsequently directly injected. Periodic measurement of tumor size revealed that a single intratumoral injection of Surv.m-CRA significantly inhibited tumor growth in comparison to Ad. dE1.3 42 days after adenoviral injection (Figure 8A, B). By contrast, there was no significant difference in tumor size on day 42 between the controls, *i.e.*, Ad.dE1. 3–treated and PBS–treated mice. Furthermore, histopathologic analysis of viable and dead tumor cells clearly demonstrated the potent therapeutic effects of Surv.m-CRAs beyond what could be shown by the macroscopic analysis (Figure 8B, C): the macroscopically large tumor nodules in control mice treated with either Ad.dE1.3 or

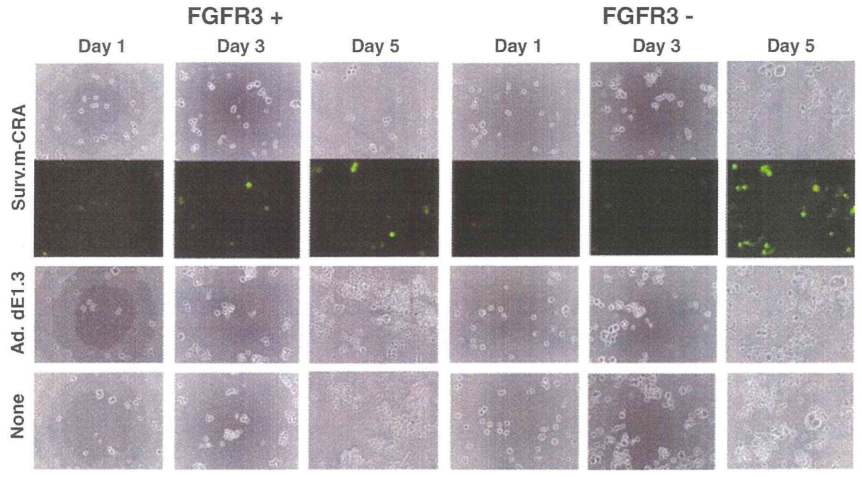

Figure 7 Viral replication of Surv.m-CRA and cytotoxicity against sorted FGFR3-positive and FGFR3-negative cells. Sorted FGFR3-positive and FGFR3-negative cells were infected with Surv.m-CRA, Ad.dE1.3, or no virus (none) at an MOI of 1. The cells were observed under phase-contrast and fluorescence microscopy 1, 3, and 5 days after infection. Representative phase-contrast (upper) and fluorescence (lower) images are shown at 50× magnification. In the case of no infection (none), FGFR3-positive cells proliferated more rapidly than FGFR3-negative cells after 3 and 5 days. By contrast, the proportion of remaining cells 5 days after Surv.m-CRA infection was lower in FGFR3-positive than in FGFR3-negative cells. These results suggest that Surv.m-CRA exhibited more efficient replication in and cytotoxicity against sorted FGFR3-positive than FGFR3-negative cells.

PBS consisted mainly of viable tumor cells with histological features of active malignancy, including a large number of mitoses, heterogeneous morphologies of nuclei and cells, and densely accumulated cells; in addition, these tumors contained small and spotty areas consisting of spontaneous necroses in their centers (Figure 8B, C). By contrast, the macroscopically small nodules in the Surv.m-CRA–treated mice consisted histologically of large necrotic areas with loose connective tissues but no apparent viable malignant cells. Thus, a single injection of Surv.m-CRA into tumor nodules generated by implantation of RSC-enriched rhabdomyosarcoma cells in mice exhibited a potent therapeutic effect *in vivo*.

Discussion

We previously showed that Surv.m-CRAs could treat a broad range of cancer types more efficiently and safely (*i.e.*, cancer-specifically) than Tert.m-CRAs, which are among the best CRAs [11,12,25]. The results of this study demonstrate not only that Surv.m-CRAs can efficiently kill all populations of rhabdomyosarcoma cells, including both RSCs and their progeny (*i.e.*, the bulk of malignant cells), but also that the antitumor effects of Surv.m-CRAs are higher against RSCs. This feature is clinically meaningful and promising because the therapeutic mode of Surv.m-CRAs is opposite to that of conventional chemoradiotherapies, and because Surv.m-CRA may overcome, at least in part, the serious drawbacks of current cancer treatments.

Some previous studies assessed the cytotoxic effects of oncolytic viruses on CSCs [26], and several groups reported that their CRAs might be effective against stem-like cancer cells of glioblastoma [27,28], esophageal cancer [29], and breast cancer [30]. However, the efficacy of these CRAs against CSCs was not accurately established in these studies, due to limitations of the analyses or the CSC models used. From the standpoint of the analyses, the lack of point-by-point comparisons of biological features, both regarding genes that regulated viral replication and the differences in the effects of CRAs between sorted CSCs and progeny, led to unclear conclusions regarding the most important question: how efficiently do these viruses kill CSCs in comparison to their progeny [27,28]? From the standpoint of the CSC models, some previous studies used radioresistant cancer cells as cancer stem-like cells, but did not examine sorted CSCs [28]. Although radiation treatment may enrich CSCs, the radioresistant cancer cells are not equivalent to CSCs. Thus, although the previous studies did provide some important information, their results may not allow a generalized assessment regarding the potentials of CRAs against CSCs. Therefore, the efficacy of each oncolytic virus and CRA against CSCs should be individually and carefully assessed in the proper experimental models.

To accurately assess the biological features and therapeutic potential of Surv.m-CRAs against CSCs, in a previous study we identified FGFR3 as a useful marker that allows accurate monitoring and purification of RSCs; a single implanted FGFR3-positive rhabdomyosarcoma cell could form a tumor *in vivo*, whereas FGFR3-negative

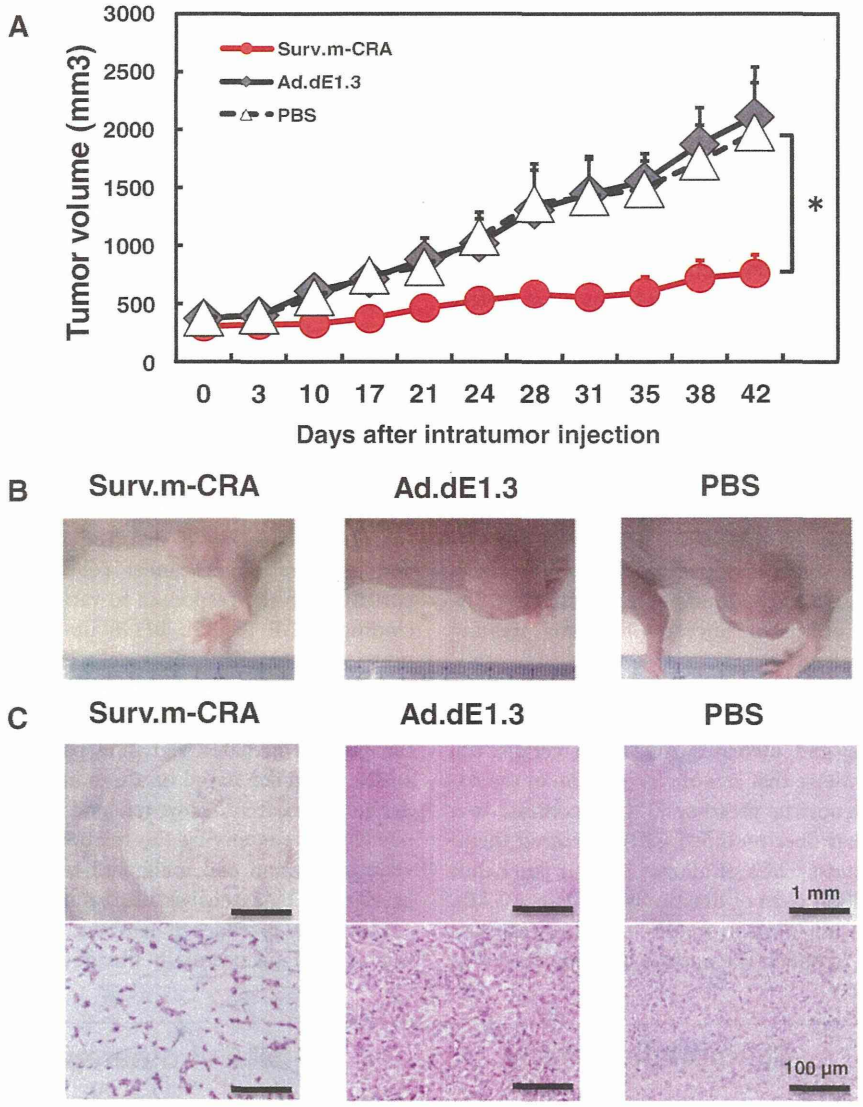

Figure 8 ***In vivo*** **therapeutic effects of Surv.m-CRA against tumors in mice.** Tumor nodules were generated in mice by implantation of RSC-enriched rhabdomyosarcoma cells, and a single intratumoral injection of Surv.m-CRA, Ad.dE1.3, or PBS was subsequently administered to each nodule. **(A)** The macroscopic tumor size after each treatment. A significant difference was found between mice treated with Surv.m-CRA and those treated with either control (Ad.dE1.3 or PBS) ($P < 0.05$). **(B)** Representative macroscopic pictures of a tumor nodule 42 days after each treatment. **(C)** Representative histopathologic pictures of hematoxylin/eosin-stained sections in the tumor nodule 42 days after each treatment. In Ad.dE1.3-treated and the PBS-treated mice, tumor nodules mainly consisted of viable tumor cells exhibiting malignant features without large necrotic areas. By contrast, in Surv.m-CRA–treated mice, tumor nodules mainly consisted of large necrotic areas with loose connective tissues and without viable tumor cells. Original magnification: 40× (top; scale bar, 1 mm) and 400× (bottom; scale bar, 100 mm).

cells did not form tumors [7]. Because FGFR3-positive rhabdomyosarcoma cells, including KYM-1 cells, were characterized as RSCs in our previous study, it was not necessary to repeat this characterization in this study. Based on those results, in this study we carefully compared the biological features of survivin (both endogenous gene expression and the transduced promoter activity) and Surv.m-CRAs, both between RSC-enriched and RSC-exiguous conditions and between purified FGFR3-positive RSCs and purified FGFR3-negative progeny cells. We used both of these experimental systems because the former (enriched CSCs together with some progeny cells) may, at least in part, reflect the *in vivo* microenvironment, whereas the latter (purified CSCs) may facilitate clarification of the biological differences between CSCs and progenitor cells. Analyses in both experimental systems

clearly revealed that the activity of the survivin promoter, which has already been shown to have stronger and more cancer-specific activity than the Tert promoter [11,12], was further increased in RSCs; indeed, Surv.m-CRAs efficiently killed all populations with the desirable property of increased therapeutic efficacy against RSCs.

On the other hand, the movements and changes of CSCs within the body are not fully understood, and these points can be accurately addressed in only a few animal models. In addition, human type 5 adenovirus, which is the backbone of Surv.m-CRAs, can infect mouse cells but cannot replicate in mice; therefore, there is no available animal model in which the therapeutic efficacy of CRAs against CSCs can be accurately analyzed. Therefore, we assessed the therapeutic efficiency of Surv.m-CRAs in tumor nodules generated by implantation of RSC-enriched rhabdomyosarcoma cells; Surv.m-CRAs exhibited a potent *in vivo* therapeutic effect in this animal model. Although the *in vivo* efficacy of Surv.m-CRAs against CSCs cannot be quantitatively assessed, this result demonstrates the therapeutic efficacy and the possible clinical utility of Surv.m-CRAs for treating rhabdomyosarcoma.

The RGD-based fiber modification allows the adenovirus to use integrins as alternative receptors during the cell entry process, and increases AGTEs in certain cell types, particularly those that lack the expression of the native Coxsackie-adenovirus receptor [31]. In contrast to a previous report that fiber-modified CRA increased therapeutic efficacy against CSCs of glioma [27], in our hands the fiber modification did not drastically increase AGTEs. Therefore, we did not need to modify the fibers of Surv.m-CRAs in order to obtain therapeutic benefits, at least in this model. The clinical utility of the fiber modification may depend on the adenoviral infectivity in each cell type.

Together with the previous findings, the results of this study suggest the possible therapeutic efficacy of Surv.m-CRAs against other types of CSCs. Clinical studies previously demonstrated that high survivin expression levels are positively correlated with poor prognosis, accelerated rate of recurrence, and increased resistance to therapy in a variety of cancer types, including rhabdomyosarcoma [5,13,14]. Our results reported here regarding up-regulated survivin expression and survivin promoter activity in RSCs are consistent with the clinical findings, and should therefore be considered reasonable. Because a close relationship between higher expression levels of survivin and more malignant phenotypes has been observed in a variety of cancer types, the potent efficacy of Surv.m-CRAs to the RSCs revealed in this study may be applicable to other types of CSCs.

In terms of mechanism, accumulated data have revealed that survivin is involved in apoptosis resistance and proliferation of cancer cells, mediated at least in part through the responses to various growth factors, including bFGF [32,33]. bFGF up-regulates survivin expression in certain cancer cells [32], and survivin plays an essential role in angiogenesis in tumors by up-regulating bFGF expression [33], leading to activation of the FGFR3-mediated signaling pathway [7]. Any mechanistic inference based on these findings would necessarily be speculative, however, and the overall molecular mechanism underlying the relationship between the survivin expression and malignant features of CSCs should be clarified by extensive future studies.

This study provides general and important information that should be useful in the development of oncolytic

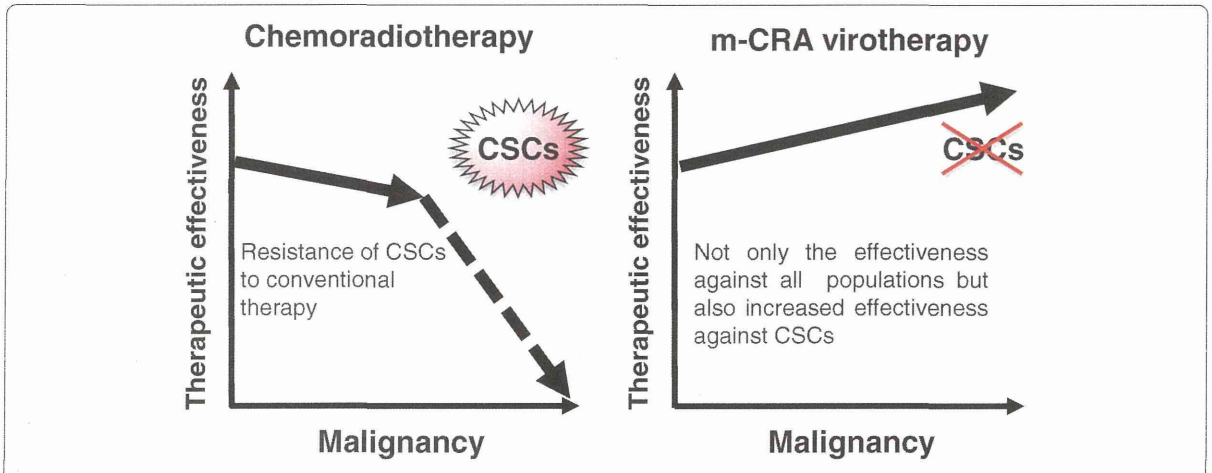

Figure 9 The putative therapeutic advantage of m-CRA virotherapy. In general, the therapeutic effectiveness of chemoradiotherapy is decreased in the advanced malignant tumor cells, and in particular, CSCs are resistant to conventional chemoradiotherapies. In contrast, not only m-CRA virotherapy can efficiently kill all populations of malignant tumor cells, including CSCs and their progeny, but also the antitumor effects of m-CRA virotherapy are higher against CSCs.

virotherapies against CSCs. To date, there have been very few successful reports of transcriptional targeting of oncolytic viruses against CSCs. In particular, none of the previous reports clearly showed that oncolytic viruses successfully acquired increased therapeutic efficacy against CSCs in parallel to increases in promoter activity and expression of a target gene. In this study, expression and promoter activity of survivin were further increased in CSCs; as a result of these transcriptional changes, Surv.m-CRAs exerted increased therapeutic efficacy against CSCs. Although the replicative mechanisms of adenoviruses have not been fully elucidated, the results described here suggest that the promising features of Surv.m-CRA may be due partly to specific features of adenoviruses and partly to the function of the survivin gene. Taken together, these findings demonstrate that Surv.m-CRA is an effective anticancer agent, but more generally, the results indicate that the use of m-CRAs represents a promising strategy for the development of effective anticancer agents against CSCs (Figure 9). In other words, the results described here pave the way to future development of several effective m-CRA–based therapies against CSCs; future progress will proceed via identification of new genes that target CSCs and generation of new m-CRAs using the promoters of these genes.

Conclusion

Surv.m-CRAs demonstrated not only therapeutic efficacy against all the populations of rhabdomyosarcoma, but also increased efficacy against RSCs. These results will facilitate the clinical application of Surv.m-CRAs, and should be useful for future development of oncolytic virotherapies that target CSCs.

Abbreviations

CSCs: Cancer stem cells; Surv.m-CRAs: Survivin-responsive conditionally replicating adenoviruses regulated with multiple factors; RSCs: Rhabdomyosarcoma stem cells; FGFR3: Fibroblast growth factor receptor 3; CRAs: Conditionally replicating adenoviruses; AGTE: The adenoviral gene transduction efficiency; IAP: Inhibitor of apoptosis; Tert.m-CRAs: Telomerase reverse transcriptase-responsive m-CRAs; bFGF: basic fibroblast growth factor; RSV promoter: Rous sarcoma virus long terminal repeat; EGFP: Enhanced green fluorescent protein; CMV: Cytomegalovirus; MOI: Multiplicities of infection; PBS: Phosphate-buffered saline.

Competing interests

K. Kosai is the founder of WyK BiotechPharma Inc., but does not earn a salary from the company. All other authors declare no competing interest.

Authors' contributions

KT and YW designed the experimental protocol, performed the most of experiments, analyzed the data, and wrote the manuscript. MI, KM, and RI performed some experiments. TS provided the materials and information regarding rhabdomyosarcoma stem cells. SK and SN partially supervised the preclinical study. KK conceived and designed the study, supervised all the experiments, assessed the data, and wrote the manuscript. All authors read and approved the final manuscript.

Acknowledgements

We thank E. Kishi for technical assistance, Dr. H. Hamada (Tokyo University of Pharmacy and Life Sciences) for providing Ad.CA-EGFP and Ad.CA-EGFP/RGD, and Dr. H. Mizuguchi (Osaka University) for providing Ad.CMV-EGFP. This work was supported by a grant for Promoting Business using Advanced Technology from the Japan Society and Technology Agency, and Health and Labor Science Research Grants for Third Term Comprehensive Control Research for Cancer from the Ministry of Health, Labour and Welfare of Japan.

Author details

[1]Department of Gene Therapy and Regenerative Medicine, Kagoshima University Graduate School of Medical and Dental Sciences, Kagoshima, Japan. [2]Department of Digestive Surgery, Breast and Thyroid Surgery, Kagoshima University Graduate School of Medical and Dental Sciences, Kagoshima, Japan. [3]The Near-Future Locomoter Organ Medicine Creation Course (Kusunoki Kai), Kagoshima University Graduate School of Medical and Dental Sciences, Kagoshima, Japan. [4]Department of Orthopaedic Surgery, Kagoshima University Graduate School of Medical and Dental Sciences, Kagoshima, Japan.

Received: 18 October 2013 *Accepted:* 22 January 2014
Published: 27 January 2014

References

1. Rasheed ZA, Kowalski J, Smith BD, Matsui W: **Concise review: emerging concepts in clinical targeting of cancer stem cells.** *Stem Cells* 2011, **29**:883–887.
2. Yu Z, Pestell TG, Lisanti MP, Pestell RG: **Cancer stem cells.** *Int J Biochem Cell Biol* 2012, **44**:2144–2151.
3. Arai F, Hirao A, Ohmura M, Sato H, Matsuoka S, Takubo K, Ito K, Koh GY, Suda T: **Tie2/angiopoietin-1 signaling regulates hematopoietic stem cell quiescence in the bone marrow niche.** *Cell* 2004, **118**:149–161.
4. Soltanian S, Matin MM: **Cancer stem cells and cancer therapy.** *Tumour Biol* 2011, **32**:425–440.
5. Wang C: **Childhood rhabdomyosarcoma: recent advances and prospective views.** *J Dent Res* 2012, **91**:341–350.
6. Kawabata N, Ijiri K, Ishidou Y, Yamamoto T, Nagao H, Nagano S, Maeda S, Komiya S, Setoguchi T: **Pharmacological inhibition of the Hedgehog pathway prevents human rhabdomyosarcoma cell growth.** *Int J Oncol* 2011, **39**:899–906.
7. Hirotsu M, Setoguchi T, Matsunoshita Y, Sasaki H, Nagao H, Gao H, Sugimura K, Komiya S: **Tumour formation by single fibroblast growth factor receptor 3-positive rhabdomyosarcoma-initiating cells.** *Br J Cancer* 2009, **101**:2030–2037.
8. Alemany R, Balague C, Curiel DT: **Replicative adenoviruses for cancer therapy.** *Nat Biotechnol* 2000, **18**:723–727.
9. Lomonosova E, Subramanian T, Chinnadurai G: **Requirement of BAX for efficient adenovirus-induced apoptosis.** *J Virol* 2002, **76**:11283–11290.
10. Nagano S, Oshika H, Fujiwara H, Komiya S, Kosai K: **An efficient construction of conditionally replicating adenoviruses that target tumor cells with multiple factors.** *Gene Ther* 2005, **12**:1385–1393.
11. Horikawa Y, Wang Y, Nagano S, Kamizono J, Ikeda M, Komiya S, Kosai KI: **Assessment of an altered E1B promoter on the specificity and potency of triple-regulated conditionally replicating adenoviruses: implications for the generation of ideal m-CRAs.** *Cancer Gene Ther* 2011, **18**:724–733.
12. Kamizono J, Nagano S, Murofushi Y, Komiya S, Fujiwara H, Matsuishi T, Kosai K: **Survivin-responsive conditionally replicating adenovirus exhibits cancer-specific and efficient viral replication.** *Cancer Res* 2005, **65**:5284–5291.
13. Altieri DC: **Survivin, versatile modulation of cell division and apoptosis in cancer.** *Oncogene* 2003, **22**:8581–8589.
14. Fukuda S, Pelus LM: **Survivin, a cancer target with an emerging role in normal adult tissues.** *Mol Cancer Ther* 2006, **5**:1087–1098.
15. Terazaki Y, Yano S, Yuge K, Nagano S, Fukunaga M, Guo ZS, Komiya S, Shirouzu K, Kosai K: **An optimal therapeutic expression level is crucial for suicide gene therapy for hepatic metastatic cancer in mice.** *Hepatology* 2003, **37**:155–163.
16. Yuge K, Takahashi T, Nagano S, Terazaki Y, Murofushi Y, Ushikoshi H, Kawai T, Khai NC, Nakamura T, Fujiwara H, Kosai K: **Adenoviral gene transduction of hepatocyte growth factor elicits inhibitory effects for hepatoma.** *Int J Oncol* 2005, **27**:77–85.
17. Nagano S, Yuge K, Fukunaga M, Terazaki Y, Fujiwara H, Komiya S, Kosai K: **Gene therapy eradicating distant disseminated micro-metastases by optimal cytokine expression in the primary lesion only: novel concepts for successful cytokine gene therapy.** *Int J Oncol* 2004, **24**:549–558.

18. Ushikoshi H, Takahashi T, Chen X, Khai NC, Esaki M, Goto K, Takemura G, Maruyama R, Minatoguchi S, Fujiwara T, *et al*: **Local overexpression of HB-EGF exacerbates remodeling following myocardial infarction by activating noncardiomyocytes.** *Lab Invest* 2005, **85**:862–873.
19. Dehari H, Ito Y, Nakamura T, Kobune M, Sasaki K, Yonekura N, Kohama G, Hamada H: **Enhanced antitumor effect of RGD fiber-modified adenovirus for gene therapy of oral cancer.** *Cancer Gene Ther* 2003, **10**:75–85.
20. Takahashi T, Kawai T, Ushikoshi H, Nagano S, Oshika H, Inoue M, Kunisada T, Takemura G, Fujiwara H, Kosai K: **Identification and isolation of embryonic stem cell-derived target cells by adenoviral conditional targeting.** *Mol Ther* 2006, **14**:673–683.
21. Murofushi Y, Nagano S, Kamizono J, Takahashi T, Fujiwara H, Komiya S, Matsuishi T, Kosai K: **Cell cycle-specific changes in hTERT promoter activity in normal and cancerous cells in adenoviral gene therapy: a promising implication of telomerase-dependent targeted cancer gene therapy.** *Int J Oncol* 2006, **29**:681–688.
22. Kawai T, Takahashi T, Esaki M, Ushikosi H, Nagano S, Fujiwara H, Kosai K: **Efficient cardiomyogenic differentiation of embryonic stem cell by fibroblast growth factor 2 and bone morphogenetic protein 2.** *Circ J* 2004, **68**:691–702.
23. Ikoma T, Takahashi T, Nagano S, Li YM, Ohno Y, Ando K, Fujiwara T, Fujiwara H, Kosai K: **A definitive role of RhoC in metastasis of orthotopic lung cancer in mice.** *Clin Cancer Res* 2004, **10**:1192–1200.
24. Fukunaga M, Takamori S, Hayashi A, Shirouzu K, Kosai K: **Adenoviral herpes simplex virus thymidine kinase gene therapy in an orthotopic lung cancer model.** *Ann Thorac Surg* 2002, **73**:1740–1746.
25. Nemunaitis J, Tong AW, Nemunaitis M, Senzer N, Phadke AP, Bedell C, Adams N, Zhang YA, Maples PB, Chen S, *et al*: **A phase I study of telomerase-specific replication competent oncolytic adenovirus (telomelysin) for various solid tumors.** *Mol Ther* 2010, **18**:429–434.
26. Friedman GK, Cassady KA, Beierle EA, Markert JM, Gillespie GY: **Targeting pediatric cancer stem cells with oncolytic virotherapy.** *Pediatr Res* 2012, **71**:500–510.
27. Jiang H, Gomez-Manzano C, Aoki H, Alonso MM, Kondo S, McCormick F, Xu J, Kondo Y, Bekele BN, Colman H, *et al*: **Examination of the therapeutic potential of Delta-24-RGD in brain tumor stem cells: role of autophagic cell death.** *J Natl Cancer Inst* 2007, **99**:1410–1414.
28. Nandi S, Ulasov IV, Tyler MA, Sugihara AQ, Molinero L, Han Y, Zhu ZB, Lesniak MS: **Low-dose radiation enhances survivin-mediated virotherapy against malignant glioma stem cells.** *Cancer Res* 2008, **68**:5778–5784.
29. Zhang X, Komaki R, Wang L, Fang B, Chang JY: **Treatment of radioresistant stem-like esophageal cancer cells by an apoptotic gene-armed, telomerase-specific oncolytic adenovirus.** *Clin Cancer Res* 2008, **14**:2813–2823.
30. Eriksson M, Guse K, Bauerschmitz G, Virkkunen P, Tarkkanen M, Tanner M, Hakkarainen T, Kanerva A, Desmond RA, Pesonen S, Hemminki A: **Oncolytic adenoviruses kill breast cancer initiating CD44 + CD24-/low cells.** *Mol Ther* 2007, **15**:2088–2093.
31. Nakamura T, Sato K, Hamada H: **Effective gene transfer to human melanomas via integrin-targeted adenoviral vectors.** *Hum Gene Ther* 2002, **13**:613–626.
32. Cosgrave N, Hill AD, Young LS: **Growth factor-dependent regulation of survivin by c-myc in human breast cancer.** *J Mol Endocrinol* 2006, **37**:377–390.
33. Wang P, Zhen H, Zhang J, Zhang W, Zhang R, Cheng X, Guo G, Mao X, Wang J, Zhang X: **Survivin promotes glioma angiogenesis through vascular endothelial growth factor and basic fibroblast growth factor *in vitro* and *in vivo*.** *Mol Carcinog* 2011, **51**:586–595.

doi:10.1186/1479-5876-12-27
Cite this article as: Tanoue *et al.*: Survivin-responsive conditionally replicating adenovirus kills rhabdomyosarcoma stem cells more efficiently than their progeny. *Journal of Translational Medicine* 2014 12:27.

CellBio, 2013, 2, 179-185
Published Online December 2013 (http://www.scirp.org/journal/cellbio)
http://dx.doi.org/10.4236/cellbio.2013.24020

Scientific Research

Immunohistochemical Analysis of the Acid Secretion Potency in Gastric Parietal Cells

Rie Irie-Maezono[1], Shinichiro Tsuyama[2]
[1]Department of Gene Therapy and Regenerative Medicine, Kagoshima University, Graduate School of Medical and Dental Sciences, Kagoshima, Japan
[2]Laboratory for Neuroanatomy, Kagoshima University, Graduate School of Medical and Dental Sciences, Kagoshima, Japan
Email: maezono@m.kufm.kagoshima-u.ac.jp

Received July 31, 2013; revised August 31, 2013; accepted September 7, 2013

ABSTRACT

Gastric parietal cells are important in acid secretion, but it is unclear which cells throughout the gastric gland have the highest secretion potency. Here, we used immunohistochemical methods with anti-H^+, K^+-ATPase, phosphoryl ezrin and CD44 antibodies to study the distribution of gastric acid secretion activity. Stomach tissues from freely fed and starved rats were cryofixed for light microscopy or fixed by high-pressure freezing for electron microscopy. Parietal cells from freely fed animals corresponded to the active secretion phase and to the inactive resting phase from starved rats. Anti-H^+, K^+-ATPase and anti-phosphoryl ezrin labeling were observed on the membrane of the intracellular canaliculi and the tubulovesicle from freely fed rats, while cells from starved animals showed weak labeling with anti-phosphoryl ezrin antibody staining. Morphometrical analysis at the electron microscopic level was performed on active and inactive acid secretory phases between the upper and base regions of the gland. H^+, K^+-ATPase and CD44 were distributed on both sites of the microvillous and tubulovesicle membrane in the same cells, but phosphoryl ezrin localized predominantly on the microvillous membrane in active cells of the glandular neck and upper base. Therefore, the highest secreting potency appeared to be in cells of the glandular neck and upper base.

Keywords: Gastric Parietal Cells; Secretory Potency; Phosphoryl Ezrin; Histochemical Morphometry

1. Introduction

Gastric parietal cells play a major role in acid secretion and are widely distributed from the pit to the base of rat gastric glands. They show characteristic aspects of intracellular canaliculi (IC) with numerous microvilli and tubulovesicles (TV) in the cytoplasm, which are thought to be interconvertable structures. Although the conversion mechanism for these structures is unclear, various hypothesizes have been proposed. During the active acid-secreting phase of parietal cells, the IC is markedly expanded, but the cells undergo a morphological transformation during their inactive resting phase when the IC reduces in width and the TV mass increases [1,2]. The secretion activity alternates according to the physiological phases of feeding or starving.

Proton potassium ATPase (H^+, K^+-ATPase; "the proton pump") is an important enzyme for gastric acid secretion and exists as an integral membrane-protein along the IC and TV throughout the parietal cell membrane. We previously used high-pressure freezing followed by freeze-substitution to investigate the histochemistry of gastric gland cells and the ultrastructural alterations that occur in both fed and starved phases [3,4]. Cryofixation using rapid freezing (especially high pressure rapid freezing for capable freezing depth) is believed to be superior to conventional chemical fixation with regard to morphological preservation and retention of soluble components. Using antibodies against the proton potassium ATPase α- and β-subunits, we also showed that the enzyme localized on both IC and TV membranes in almost all parietal cells throughout the length of the gland [3-5].

Parietal cells contain more actin than other glandular cells. Transformation between IC and TV occurs with redistribution of actin in the cell. Filamentous actins are anchored to the plasma membrane via phosphoryl ezrin,

and most actin molecules are thought to form a globular structure in the inactive resting state, which molecules polymerize rapidly to form a filamentous structure upon active acid secretion [2,6-11]. Ezrin is a member of the ERM (ezrin/radixin/moesin) family of proteins that is implicated in linking functional activities of the plasma membrane to the actin cytoskeleton. In addition, actin binds to intramembranous CD44 via phosphoryl ezrin in the plasma membrane [12-14]. It has previously been suggested that the above-mentioned morphological changes are induced and triggered by this cytoskeletal reorganization of β-actin [15-17].

The purpose of the present study was to investigate which parietal cells are more active than others in terms of acid secretion, based on the distribution of phosphoryl ezrin and CD44 throughout the gland using immunohistochemical techniques.

2. Materials and Methods

2.1. Tissue Preparation

Ten male Wistar rats were used in the experiments and divided into two groups of five animals each. One group was fed freely and the other was starved for 48 h with free access to water. The rats were anesthetized with an intraperitoneal injection of sodium pentobarbital, and the pH of the luminal gastric juice was determined. The stomach tissues were cut into small pieces and cryofixed using a rapid freezing device (RF-6, Eiko, Japan) using liquid propane for cryofixing and liquid nitrogen for light microscopy. The specimens were then freeze-substituted with acetone containing 0.2% glutaraldehyde at −79°C for 72 h and embedded in paraffin [17].

For electron microscopy, the specimens underwent high-pressure freezing under a 21×10^5 hPa atmosphere (HPM 010, BAL-TEC, Liechtenstein). The frozen specimens were freeze-substituted with acetone containing 1% osmium tetroxide or 0.2% glutaraldehyde at −79°C for 72 h and were embedded in Epon812 or Lowicryl K4M resin, respectively [3].

2.2. Primary and Secondary Antibodies

A rabbit antibody against the H^+, K^+-ATPase (proton pump) α-subunit (Immunogen; C-terminal synthetic peptide based on the porcine H^+, K^+-ATPase α-subunit sequence) was purchased from Calbiochem-Novabiochem (San Diego, CA). The antibody was used at a dilution of 1:100 in phosphate buffered saline (PBS). A mouse monoclonal antibody against the H^+, K^+-ATPase β-subunit (Immunogen; purified 34-kDa core peptide from deglycosylated hog gastric microsomes) was purchased from Abcam Ltd. (Cambridge, UK) and diluted 1:200 in PBS. A rabbit polyclonal antibody against phosphoryl ezrin (Immunogen: KLH-conjugated, synthetic phosphopeptide corresponding to residues surrounding Thr567 of human ezrin) and an anti-CD44 antibody were purchased from CHEMICON International, Inc. (Temecula, CA). These were used at a dilution of 1: 10 - 20 in PBS. A mouse monoclonal antibody against actin (pan Ab-5; Clone ACTN05) was purchased from LAB VISION Co. (Fremont, CA). This antibody reacts with all six known isoforms of vertebrate actin (MW-42 kD) and also with two highly homologous cytoplasmic actins (β, γ). This antibody was diluted 1: 10 - 80 in PBS. The antibodies were confirmed to show cross-reactivity against the rat. The following were used as secondary antibodies: biotinylated goat anti-mouse immunoglobulin ($F(ab')_2$) or biotinylated swine anti-rabbit immunoglobulin (DAKO Cytomation, Glostrup, Denmark) diluted 1: 100 - 200 in PBS; horseradish peroxidase (HRP)-conjugated streptavidin (DAKO Cytomation) (1:200 in Tris-buffered-saline; TBS); colloidal gold (CG)-conjugated streptavidin (1:1 in PBS) from British BioCell International (Cardiff, UK).

2.3. Immunohistochemical Staining for Light Microscopy

Specimens embedded in paraffin were cut into 4 μm-thick slices with a sliding Jung-model microtome, mounted on silconized glass slides and air-dried. Sections were deparaffinized, rehydrated and immersed in PBS. After blocking endogenous peroxidase activity with 0.3% hydrogen peroxide in methanol, specimens were incubated with primary antibodies against the H^+, K^+-ATPase α- and β-subunits. They were then labeled with biotinylated anti-rabbit or anti-mouse IgG antibodies overnight followed by HRP-conjugated streptavidin for 1 h. Visualization was performed using 3, 3'-diaminobenzidine tetrahydrochloride (DAB; DAKO Cytomation) for 10 min. Finally, sections were rinsed in distilled water, counterstained with Mayer's hematoxylin, dehydrated in a graded ethanol series, cleared in xylene and mounted with Eukitt (O. Kindler, Germany).

2.4. Electron Microscopy

Ultrathin sections from specimens fixed with 1% osmium tetroxide and embedded in epoxy resin were cut with a Reichert Ultracat-N ultramicrotome and stained with uranyl acetate and Reynolds' lead citrate. They were observed using a HITACHI H-7000 electron microscope at an acceleration voltage of 80 kV.

Specimens fixed with 0.2% glutaraldehyde and embedded in Lowicryl K4M resin were stained by the immunogold method (particle size of colloidal gold (CG): 15 nm and 10 nm). Thin sections were incubated with unlabeled-streptavidin (Southern Biotech, Birmingham, AL) for 30 min at room temperature to block endogenous

biotin. Immunogold staining was performed as described previously [4,18]. Briefly, the sections were incubated with anti-H^+, K^+-ATPase α- and β-subunits, anti-phosphoryl ezrin and anti-CD44 antibodies followed by biotinylated anti-rabbit or anti-mouse IgG antibodies and labeled with streptavidin-colloidal gold. Finally, the sections were counterstained with uranyl acetate and Millonig's lead acetate.

2.5. Morphometrical Analysis of Labeling Density with Phosphoryl Ezrin Immunogold Staining

The parietal cell labeling density with the anti-phosphoryl ezrin antibody was analyzed using Image-J NIH software. Thus, the labeling number of gold particles (on IC containing multiple microvilli) was counted on electron microscopic photographs taken at 15,000 × magnification of the neck or base region (n = 20 each) of active phase glands (fed animals) and inactive resting phase glands (starved animals). The labeling density was estimated as the number of gold particles per unit area (μm^2) of IC. For the assessment of the phosphoryl ezrin labeling-density, the results were statistically analyzed by *t*-test using Microsoft Excel software. Statistical comparisons were made between the neck and the base area of the gland, and between active versus inactive glands from starved animals. The differences between sites or feeding/starving were evaluated by *t*-test. $P < 0.01$ or 0.05 was considered significant. The results are expressed as the arithmetic mean ± SE.

3. Results

3.1. Morphological Observation

The average pH in the fed rats was 2.0, compared with 6.4 in the starved rats. We therefore hypothesized that the former corresponds to the active phase and the latter to the inactive resting phase of gastric juice secretion.

The parietal cells showed excellent ultrastructural preservation at the electron microscopic level. The ultrastructure of IC, TV, and other organelles was well preserved for each active and inactive phase of glands when specimens were processed successfully by means of HPF-followed by FS.

3.2. Immunohistochemical Observation with Anti-H^+, K^+-ATPase Antibody

The parietal cells were labeled intensely and clearly by immunohistochemical staining with the H^+, K^+-ATPase anti-α- and -β-subunit antibodies. Cells in the neck and upper base were labeled particularly strongly in active phase animals. Staining was evenly distributed from the deep pit to the glandular base of the cells (**Figures 1(A)** and **(B)**), and the staining pattern was similar between the anti-β-subunit antibody and α-subunit antibody (data not shown). In the active phase, the microvillous membrane and apical cell membrane of the IC were labeled with the anti-α- and -β-H+, K+-ATPase subunit antibodies and with the anti-phosphorylated-ezrin antibody (corresponding to residues surrounding Thr566 and 567), while TV membranes were hardly stained. In the inactive phase, IC microvilli were labeled weakly with this antibody. The anti-CD44 antibody staining pattern was similar to that of anti-α- (and -β-) H^+, K^+-ATPase subunit antibodies in inactive phase animals (**Figures 2, 3(A)** and **(B)**). A regional labeling difference was evident from the neck to the upper base and lower base.

3.3. Morphometric Analysis with Anti-Phosphoryl Ezrin Antibody and Immunogold Labeling

Immunogold staining was performed to examine the intracellular distribution and the labeling density of the

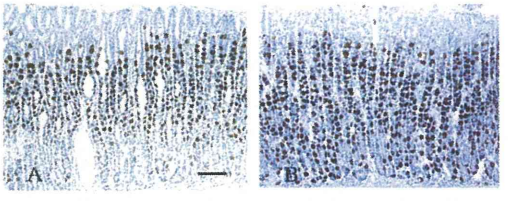

Figure 1. Active phase rat gastric gland immunostained with the anti-H^+, K^+-ATPase α-subunit antibody. (A) Parietal cells throughout the gland are stained strongly. Cells are large and plump and become smaller and more slender as they migrate downwards. Reaction products are thread-like in shape; (B) Inactive resting phase gland with similar staining. Parietal cells scattered throughout the gland are also stained positively and reaction products were observed diffusely in the cytoplasm. Scale bar = 100 μm.

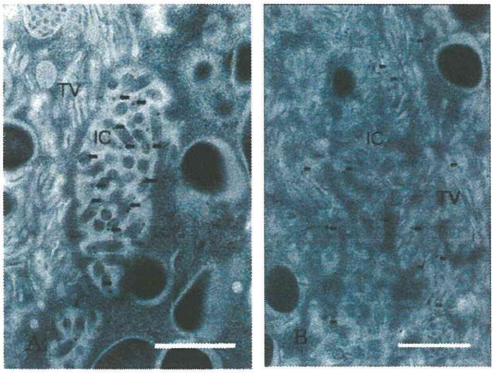

Figure 2. Section of parietal cells stained with immunogold method. (A) Anti-phosphoryl ezrin antibody staining. The IC membrane and its microvilli were stained with anti-phosphoryl ezrin antibody, but little staining was visible on the TV membrane; (B) Anti-CD44 ant-ibody staining. The two organelles (IC and TV) were labeled with this antibody. Scale bar = 1 μm.

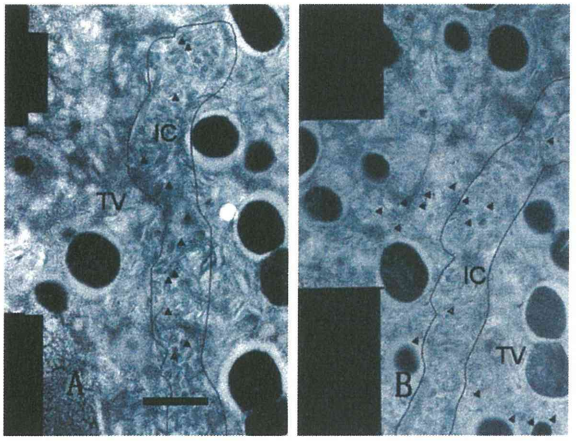

Figure 3. Adjacent serial sections immunostaining. Each photograph is composed of several distinct pictures (montaged pictures) and serially sectioned. Labeled gold particles are shown with arrowheads. The anti-phosphoryl ezrin antibody bound only to the IC microvilli (A), while the anti-CD44 antibody labeled both the IC and TV (B). Scale bar = 1 μm.

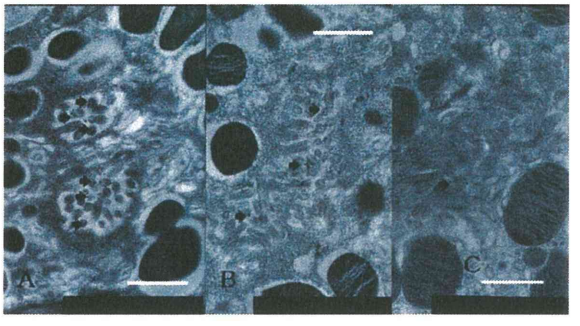

Figure 4. Labeling differences in each level of gland of parietal cell stained with immunogold using anti-phosphoryl ezrin antibody. (A) Neck region, adjoining mucous neck cell in active animals; (B) Lower region of base, neighboring chief cell; (C) Neck region from starved rats. Anti-phosphoryl ezrin antibody labeling is strong on IC membrane of parietal cell from fed (active secreting) rats (A), and moderate to weak in lower half of base (B) and through gland from starved (inactive resting or inactive secreting) rats (C). Scale bar = 1 μm.

anti-phosphoryl ezrin antibody in each cell between the gland segments. Parietal cells adjacent to mucous neck cells or chief cells were deemed to be in the neck or base region, respectively. The gold particle numbers were compared between the neck and the base region of the glands, and between active and inactive resting glands (**Figure 4**). The number of labeled gold particles was divided by the IC area to give the labeling density (per μm^2). Labeling density zonation was clear from the neck to the base, with a significantly higher density in parietal cells located in the isthmus to neck region (mean ± SE; 25.501 ± 3.736 μm^2) compared with the glandular lower base (17.082 ± 7.275 μm^2) or from inactive starved rats (1.926 ± 0.465 μm^2) (**Figures 5(A)** and **(B)**).

Statistical analysis using IMAGE-J revealed that phosphoryl ezrin expression in the neck and upper base was significantly higher than that in lower base (25.501 ± 3.736 vs 17.082 ± 7.275, $p < 0.05$) and than that in starved gland (25.501 ± 3.736 vs 1.926 ± 0.465, $p < 0.01$). These findings suggest that the phosphoryl ezrin assemble in the membrane of active parietal microvilli at neck to upper base.

4. Discussion

The component cells of gastric glands include pit mucous cells, progenitor cells, parietal cells, mucous neck cells, chief cells and endocrine cells and have previously been studied in rodents. These cells undergo mitosis in the isthmus, from where they migrate and differentiate along the longitudinal axis of the gland in an upward or downward direction [19-21]. The parietal cells migrate upwards and downwards then mature, while chief cells derive from the mucous neck cell through an intermediate cell type to the mature chief cell in a downwards migration [17]. Parietal cells adjoining the mucous neck cell are considered to be in the neck region and those next to the chief cell are in the base region of the gland.

Gastric juice is very acidic, with a pH of around 1.5. The average pH value measured in this study was pH 2.0 in fed rats and pH 6.4 in starved animals, indicating that the parietal cells of fed rats correspond to cells in the active secretory-phase, while those of starved animals correspond to cells in the inactive resting phase. The pa-

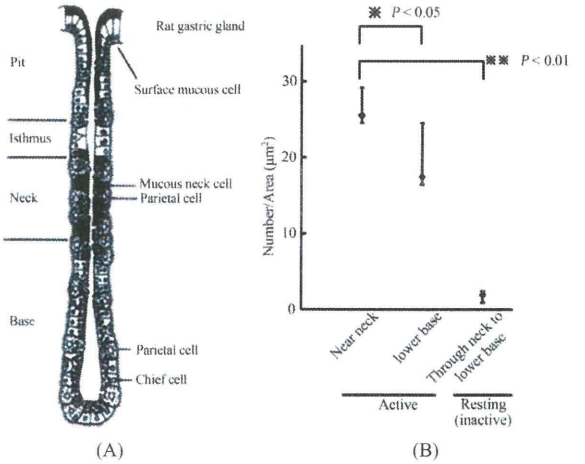

Figure 5. (A) Schematic drawing of rat gastric gland. After proliferation in the glandular isthmus, the parietal cell migrates and differentiate through neck to base of gland; (B) Statistical analysis of phosphoryl-ezrin plotting. The labeling of the cell in the near neck site was significantly higher than that in the lower base, or whole site of the gland in the resting (the inactive).